First-principles studies of electronic properties in a Pt_2CdSe_3/Pt_2HgSe_3 Kane-Mele heterobilayer

G. Santos-Castro [1,*] I. Guilhon [2,†] and J. M. Pereira, Jr. [1,‡]

[1]*Grupo de Teoria da Matéria Condensada, Departamento de Física, Universidade Federal do Ceará, 60455-760 Fortaleza, Ceará, Brazil*
[2]*Grupo de Materiais Semicondutores e Nanotecnologia, Instituto Tecnológico de Aeronáutica, DCTA, 12228-900 São José dos Campos, Brazil*

(Received 1 August 2022; revised 12 December 2022; accepted 25 January 2023; published 17 February 2023)

In this paper, we investigate the electronic band structure and optical conductivity of a Pt_2CdSe_3/Pt_2HgSe_3 heterobilayer system composed of two-dimensional jacutingaitelike materials. These layered crystals have shown interesting properties both in bulk as well as in single layers. By using first-principles density functional theory calculations and maximally localized Wannier functions, we show how the electronic and optical properties can be controlled by means of external electric fields. We found that such perturbations can lead to significant changes in the band structure, which are dependent on the orientation of the perpendicular field. In addition, the sign of the Berry curvature around the K and K' points is dependent on the magnitude and orientation of the external electric field. We also studied the topological character of the structure and found it presents quantum valley Hall states. The sizable band gap in the valley region can be used to manipulate the valley quantum freedom. Moreover, we obtained a strong anisotropy in optical conductivity, where the out-of-plane optical absorption edge is blueshifted with respect to its in-plane counterpart and the application of electric field modifies both intensities and peak positions.

DOI: 10.1103/PhysRevB.107.085418

I. INTRODUCTION

Materials that consist of single or few crystal layers can display a wide variety of interesting physical properties [1–4]. These range from insulators (hBN) to semimetals (graphene) and semiconductors [transition metal dicalchogenides (TMDs)], with some presenting unusual features, such as strong anisotropy (phosphorene) and superconductivity (twisted bilayer graphene) [2,5–8]. Recently, some of these two-dimensional (2D) materials have been shown to display topological properties, which are related to the presence of strong spin-orbit coupling and characterized by topological invariants [9–11]. Some of these topological properties are manifest in the electronic transport, as in the case of topological insulators. These are characterized by having an insulator character in the bulk region, whereas their surfaces and/or edges support conducting states [12,13]. Such states are robust against perturbations, with a degree of robustness that depends on the physical mechanism that gives rise to such states, and whether they are protected by symmetries [14,15].

A class of topological conducting states are quantum spin Hall (QSH) systems, which are insensitive to nonmagnetic perturbations [9,11]. In 2D QSH insulators (QSHIs) the edges of the system support a single scattering channel, with backscattering forbidden by time-reversal symmetry [9]. When the coupling between the layers of 2D materials with QSH states is negligible, an odd-even oscillation of topological triviality dependent on the number of layers occurs [15,16]. Also, there are topological conducting states protected by valley symmetry, called quantum valley Hall (QVH) states, which originate as a result of broken space inversion symmetry and they are robust against nonmagnetic perturbations and intervalley scattering [17–19]. In this quantum state, electrons with different valley indices move along opposite transverse edges in the presence of an in-plane electric field [20]. Systems that have these states are considered to be promising for applications in electronics, spintronics, valleytronics, and quantum information processing [11,21].

Honeycomb lattice materials, such as graphenelike 2D systems, present multiple energy valleys located at the K and K' points in the Brillouin zone [22]. It has been demonstrated that the absence of inversion symmetry in a honeycomb lattice leads to valley contrasted optical selection rules for interband transitions [17]. More recently, a family of 2D materials has been investigated for its topological properties, with the most prominent example of these being a naturally occurring mineral and honeycomb structure known as jacutingaite [23–25].

Jacutingaite (Pt_2HgSe_3, $Z = 2$) is a species of platinum-group layered mineral with an excellent {001} cleavage, which is composed of layers coupled by the van der Waals interaction in an AA configuration [25,26]. In the few-layer limit and for an odd number of layers of Pt_2HgSe_3 the system is a QSHI [27,28], whereas in the bulk limit it becomes semimetallic and dual topological, which are QSH and mirror crystalline topological [29,30]. Its structural configuration resembles a heavy metal graphene structure, with the honeycomb structure being formed by Hg atoms. As in the case of graphene, in the absence of spin-orbit coupling (SOC) there is the appearance of Dirac cones in the K and K' points [27,28]. The Hg atoms occupy the sites of the honeycomb lattice, and bonding between the Hg atoms is mediated by the Pt atoms. There is

*giselle@fisica.ufc.br
†guilhon@ita.br
‡pereira@fisica.ufc.br

a difference in height between the two sublattices, and they are arranged in a buckled conformation similar to silicene, germane, or stanene [27,28]. As other group-IV 2D systems, jacutingaite shows both valley and spin degeneracies [31,32]. In addition, the large SOC indicates that Pt_2HgSe_3 monolayers can manifest the Kane-Mele topological phase [27]. If the inversion symmetry is broken, Pt_2HgSe_3 monolayers can present the coexistence of QSH and QVH effects, valley-spin locking such as valley spin-valve effects, and Rashba and valley Zeeman-type spin splitting [33].

It has been shown experimentally that it is possible to exfoliate single layers of jacutingaite by well-known methods such as adhesive tape, intercalation, or sonication, in addition to synthetic growth on SiO_2 and gold substrates [28]. This leads to the possibility of integrating Pt_2HgSe_3 in silicon-based devices and also producing designed van der Waals heterostructures [23,28,34,35]. Theoretical calculations of other crystals that are isostructural and isoelectronic to Pt_2HgSe_3, i.e., the jacutingaite family M_2NX_3 (where $M =$ Ni, Pd, Pt; $N =$ Zn, Cd, Hg; and $X =$ S, Se, Te), show cleavage energies in the range of other experimentally exfoliable materials (0.22–0.85 J/m^2) [23]. As a reference, graphene from a graphite structure has a cleavage energy of 0.39 ± 0.02 J/m^2 [36]. A structure based on $X =$ S can be synthesized and stabilized experimentally through specific synthesis routes and/or substrate support, while for $X =$ Se, Te the structures that present high stability and Pt-based materials are QSHI with a large topological gap (about 37–262 meV, at the Perdew-Burke-Ernzerhof level) and a lower exfoliation barrier [23].

Among the simplest of van der Waals structures of interest are heterobilayers, i.e., bilayer systems consisting of two different 2D materials coupled by van der Waals interactions. The coupling between the distinct layers modifies the band structure of the original isolated systems, and also allows one to study the effects caused by the lower symmetry of the structure compared to bilayers composed of the same material [37]. Some heterostructures were proposed with the jacutingaite family, for various purposes, as devices with improved optoelectronic and thermoelectric performances [38], and topological spintronic and valleytronic applications [32,39].

In this paper, we investigate the electronic properties of heterobilayers consisting of two 2D crystals of the jacutingaite family. One attractive feature of jacutingaite is its stability, which is evident from the fact that it occurs naturally [24]. That implies that heterostructures of materials of the jacutingaite family can benefit from that stability, while having layers that, taken individually, present distinct band structures. For a stack of M_2NX_3 with the same M and X but distinct N among layers, the structure is similar to a Kane-Mele heterostructure. From a jacutingaite bilayer Pt_2HgSe_3, we modified the Hg element of a layer for the Cd element, resulting in a Kane-Mele heterobilayer. For $N =$ Cd, Hg monolayer jacutingaite the difference in the lattice parameter and bucking is less than 0.3%. The study is based on first-principles density functional theory (DFT) calculations and maximally localized Wannier functions (MLWFs) of the band structures of the system with and without external electric fields. The paper is organized as follows: Section II presents a brief description of the computational method utilized. Section III shows the results and discussions of the electronic properties, Berry quantities, and optical conductivity, followed by a conclusion.

II. METHODS

In order to investigate the structural and electronic properties of the heterobilayers, first-principles calculations based on the DFT [40,41] were performed using the plane-wave method as implemented in the QUANTUM ESPRESSO software package [42,43]. The structural optimization was performed by using Broyden-Fletcher-Goldfarb-Shanno interactive (BFGS) to minimize the total energy calculated by DFT [44–46], with an energy threshold of 4.0×10^{-5} Ry and Hellmann-Feynman forces on each atom smaller than 4.0×10^{-5} Ry/Å. A vacuum region of 20 Å and a dipole correction were inserted to decouple the periodic images [47]. The self-consistent energy threshold was of 1.0×10^{-8} Ry, the plane-wave energy cutoff was set as 120 Ry, and the Brillouin zone is sampled by a Γ-centered $12 \times 12 \times 1$ Monkhorst-Pack grid. The generalized gradient approximation of the Perdew-Burke-Ernzerhof (GGA-PBE) functional [48] was used to describe the exchange-correlation interaction and the Tkatchenko-Scheffler dispersion correction [49] was used to include the van der Waals interaction. In order to solve Kohn-Sham equations, the valence electrons were treated explicitly while the central electrons have been replaced by the optimized norm-conserving Vanderbilt pseudopotential [50,51]. The SOC was taken into account in all the calculations. The WANNIER90 package was employed to obtain the MLWFs and to perform calculations of the Berry quantities [52–54]. The WANNIERTOOLS package was used for the calculations of topological properties and 2D electronic band structures [55]. One hundred and eighty-four bands around the Fermi level were regarded, and a threshold of 1.0×10^{-10} $Å^2$ was established for the total spread change in MLWFs in the consecutive iterations and a frozen energy window of -0.75 eV at 0.75 eV around the Fermi level was considered for the MLWF disentanglement procedure [56].

The Berry curvature $\boldsymbol{\Omega}(\mathbf{k})$ is an odd function of $\mathbf{k}$ in the presence of time-reversal symmetry and an even function in the presence of spatial inversion symmetry [15], and it is determined by

$$\Omega_z(\mathbf{k}) = -2 \sum_m \sum_{m \neq n} f_{m\mathbf{k}} \frac{\mathrm{Im}(\langle u_{m\mathbf{k}}|\hat{v}_x|u_{n\mathbf{k}}\rangle\langle u_{m\mathbf{k}}|\hat{v}_y|u_{n\mathbf{k}}\rangle)}{(\epsilon_{m\mathbf{k}} - \epsilon_{n\mathbf{k}})^2}, \quad (1)$$

where $\epsilon_{m\mathbf{k}}$ is the energy eigenvalue, $f_{m\mathbf{k}} = f(\epsilon_{m\mathbf{k}})$ is the Fermi-Dirac distribution function, and $\hat{v}_\alpha$ is the velocity operator, where α denotes Cartesian directions.

A sufficiently large frozen energy window around the gap region was contemplated to calculate the optical conductivity by the Kubo-Greenwood formula divided into two parts, viz., the Hermitian part,

$$\sigma^{\mathrm{H}}_{\mathbf{k},\alpha\alpha}(\hbar\omega) = -\frac{\pi e^2}{\hbar V_c} \sum_{n,m} (f_{m\mathbf{k}} - f_{n\mathbf{k}})(\epsilon_{m\mathbf{k}} - \epsilon_{n\mathbf{k}}) \times [A_{nm,\alpha}(\mathbf{k})]^2 \frac{1}{\pi} \mathrm{Im}\left[\frac{1}{\epsilon_{m\mathbf{k}} - \epsilon_{n\mathbf{k}} - \hbar\omega - i\eta_{nm\mathbf{k}}}\right], \quad (2)$$

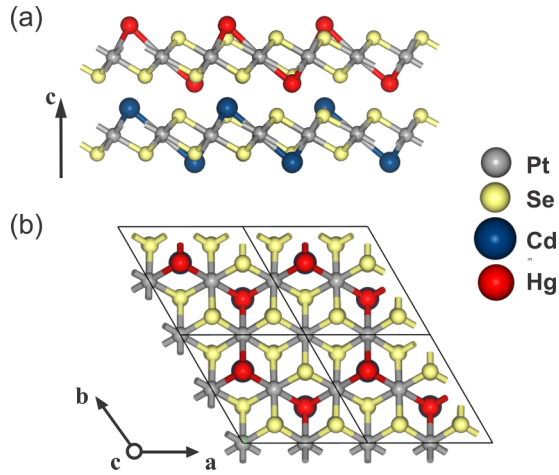

FIG. 1. (a) Profile and (b) top view of the Pt_2CdSe_3/Pt_2HgSe_3 heterobilayer. Gray, yellow, blue, and red represent platinum, selenium, cadmium, and mercury atoms, respectively. The Cd and Hg atoms, together with the Pt, form a honeycomb lattice. The unit cells are represented by solid lines.

and anti-Hermitian part,

$$\sigma^{\mathrm{AH}}_{\mathbf{k},\alpha\alpha}(\hbar\omega) = -\frac{ie^2}{\hbar V_c}\sum_{n,m}(f_{m\mathbf{k}} - f_{n\mathbf{k}}) \times \mathrm{Re}\left[\frac{\epsilon_{m\mathbf{k}} - \epsilon_{n\mathbf{k}}}{\epsilon_{m\mathbf{k}} - \epsilon_{n\mathbf{k}} - (\hbar\omega + i\eta_{nm\mathbf{k}})}\right][A_{nm,\alpha}(\mathbf{k})]^2, \tag{3}$$

where V_c is the unit cell volume, $\hbar\omega$ is the optical frequency, $A_{nm,\alpha} = \langle u_{n\mathbf{k}}|i\nabla_{\mathbf{k}\alpha}|u_{m\mathbf{k}}\rangle$ is the Berry connection, and $\eta_{nm\mathbf{k}} = \alpha|\nabla\mathbf{k}(\epsilon_{m\mathbf{k}} - \epsilon_{n\mathbf{k}})|\Delta\mathbf{k}$ is an adjustable smearing parameter with units of energy, with $\alpha = 0.03$ [57,58]. The symmetric optical conductivity tensors were calculated as follows,

$$\sigma_{\alpha\alpha} = \mathrm{Re}\,\sigma^{\mathrm{H}}_{\alpha\alpha} + i\,\mathrm{Im}\,\sigma^{\mathrm{AH}}_{\alpha\alpha}. \tag{4}$$

III. RESULTS AND DISCUSSION

We started with the structural relaxation of Pt_2CdSe_3 and Pt_2HgSe_3 monolayers. Such structures are honeycomb lattices of Cd atoms for Pt_2CdSe_3 and of Hg atoms for Pt_2HgSe_3. For both structures, the A and B sublattice sites are localized above and below, respectively, the plane of Pt atoms of the respective structures. The Pt_2CdSe_3 and Pt_2HgSe_3 monolayers have lattice parameters of 7.50 and 7.51 Å, with buckling distances of 3.42 and 3.43 Å, respectively. Both can exist as freestanding samples [23], however, our focus is on the heterostructure created by stacking these monolayers, which are coupled by van der Waals interactions, as shown in Fig. 1. The Pt_2CdSe_3/Pt_2HgSe_3 system presents a lattice constant of 7.51 Å, interlayer distance of 1.62 Å, and bucking distance in the Pt_2CdSe_3 layer of 3.64 Å and for the Pt_2HgSe_3 layer of 3.89 Å, 6.4% and 13.4% more than its isolated counterpart, respectively. In comparison with bulk Pt_2CdSe_3 and bulk jacutingaite, the interlayer distance is 1.54 and 1.55 Å, respectively, which can be explained by the stronger interlayer interaction caused by the presence of more neighboring layers. The AA stacking configuration is considered, which

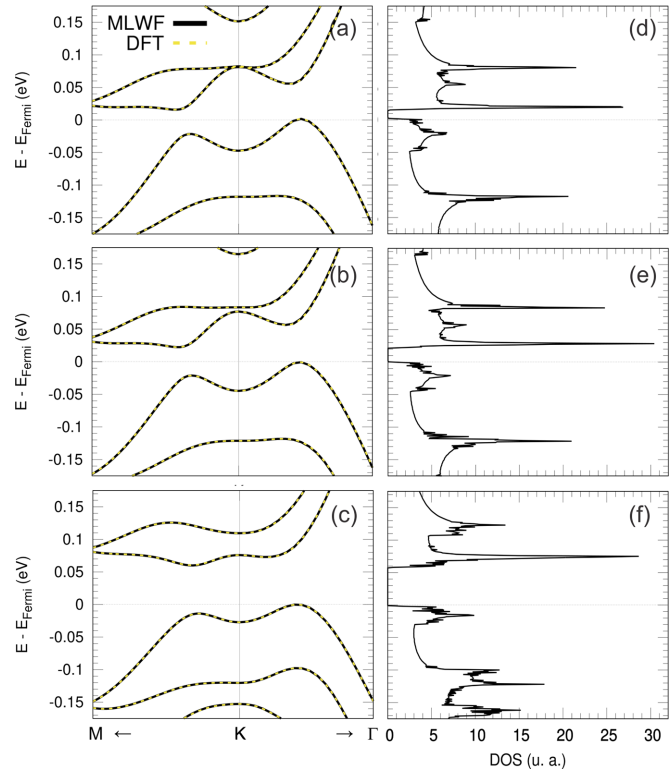

FIG. 2. Band structure and DOS for a Pt_2CdSe_3/Pt_2HgSe_3 heterobilayer (a) and (d) with an electric field of $E_{\hat{z}} = -0.5$ V/Å, (b) and (e) without an electric field, and (c) and (f) with an electric field of $E_{\hat{z}} = 0.5$ V/Å, respectively.

is similar to that of bulk jacutingaite. The structural stability was confirmed by the calculation of the binding energy (E_b) between the monolayers, defined as $E_b = E_{Pt_2CdSe_3} + E_{Pt_2HgSe_3} - E_{Pt_2CdSe_3/Pt_2HgSe_3}$ [59], where the first two terms on the right-hand side are the total energies of isolated Pt_2CdSe_3 and Pt_2HgSe_3 monolayers and the third term is the energy for the Pt_2CdSe_3/Pt_2HgSe_3 heterostructure, where we obtained $E_b = 6.34$ eV/unit cell (1.80 J/m^2). In this configuration, the bond length between Cd-Cd is reduced to 5.66 Å and between Hg-Hg is raised to 5.83 Å in relation to its respective bulk structure, with 5.70 Å (Cd-Cd) and 5.73 Å (Hg-Hg). The same behavior is found with regards to the bucking distance. For a bulk structure of Pt_2CdSe_3, the buckling distances is 3.70 Å and for Pt_2HgSe_3 is 3.75 Å.

Single layers of Pt_2CdSe_3 and Pt_2HgSe_3 are QSH Kane-Mele type of SOC semiconductors [see Figs. S1(a)– S1(d) in the Supplemental Material (SM) [60]]. For the heterobilayer composed of these monolayers, we calculated the Kohn-Sham orbitals by a first-principles approach, and following that we applied a wannierization procedure. The expectation value, density of states, state projections, Berry curvature, and optical conductivity were obtained by Wannier interpolation, which is based on the well-constructed MLWFs. As shown in Figs. 2(a)–2(c) [and also in Figs. S2(a)– S2(c) in SM [60]], the tight-binding band structure using the MLWFs shows a good agreement with the band dispersion obtained by Kohn-Sham orbitals around the band gap, confirming that the Wannier function basis is sufficiently localized and accurate.

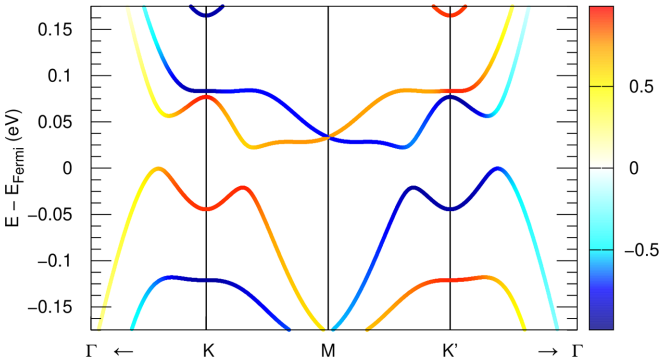

FIG. 3. Band structure of Pt_2CdSe_3/Pt_2HgSe_3 in the absence electric field. The color scheme shows the expectation value $\langle \hat{S}_z \rangle$ in units of $\hbar/2$.

For a heterobilayer Pt_2CdSe_3/Pt_2HgSe_3, in the absence of SOC, the interaction between the layers leads the energy bands hybridize, creating an indirect gap of ≈57 meV, while the respective isolated monolayers are semimetallic. The inclusion of SOC lifts the degeneracy and mixes the spin character of the bands. The effect of hybridization between monolayers is more evident and the gap is reduced. In Fig. 3, valley degeneracies and opposite spin splitting can be observed at the K and K' points due to the absence of inversion symmetry. The Γ and M points are time-reversal invariant k points, where the opposite spin states are degenerate. For the values of the electric field considered it was not possible to invert or reverse the spin polarization at the valley points [Figs. S3(a)– S3(c) in SM].

When a perpendicular electric field is applied to the heterostructure, the conduction and valence bands are modified, depending on the magnitude and direction of the field. An electric field $E_{\hat{z}} = -0.5$ V/Å reduces the gap to ≈15 meV [Fig. 2(a)], whereas for $E_{\hat{z}} = 0.5$ V/Å the gap increases to ≈60 meV [Fig. 2(c)]. For fields directed along the positive z direction, the conduction bands at the K point tend to shift apart up to about 30 meV, whereas for the negative direction the gap is reduced to zero. For the valence bands, this variation goes from 70 to 90 meV when changing the electric field from −0.5 to 0.5 V/Å. Also shown in Fig. 2 are the density of states (DOS). For an electric field $E_{\hat{z}} = -0.5$ V/Å the DOS profile is similar to the zero-field case, except for the reduction of the gap. On the other hand, for electric field $E_{\hat{z}} = 0.5$ V/Å some peaks in the conduction band in the energy range 0.02–0.08 eV are shifted to a higher energy within this same interval. There is an increase of available states at the top of the valence band with a decrease of the same at the bottom of the conduction band, which can influence transport properties significantly, also resulting in changes of the effective masses of electrons and holes.

Figure 4 shows the character of band formation by a Pt_2CdSe_3 layer for heterobilayer Pt_2CdSe_3/Pt_2HgSe_3. The results show a larger contribution of the Pt_2CdSe_3 layer for the formation of the valence bands near the Fermi level, except around the K and K' points, where a stronger hybridization increases the weight of the states associated with the Pt_2HgSe_3 layer, with the contribution around the K and K' points per layer varying with the applied electric field. For conduction bands near the Fermi energy, both layers are seen to provide similar contributions. For electric fields along the positive z direction the shift in band character and in the gap magnitude is significantly smaller than the case for an electric field in the opposite direction. We assumed electric fields in the range of $E_{\hat{z}} = -0.5$–0.5 V/Å which raised the contribution of the Pt_2HgSe_3 layer around the K point in the valence band and reduced it in the conduction band. There is a resistance to the displacement of the electronic charge density from the Pt_2CdSe_3 layer to the Pt_2HgSe_3 one, but it does not occur in the opposite direction. Therefore, for an electric field along positive z, the contribution of the Pt_2CdSe_3 increases.

For Pt_2CdSe_3 and Pt_2HgSe_3 monolayers both time-reversal and inversion symmetries are present and thus the Berry curvature $\mathbf{\Omega}(\mathbf{k})$ vanishes. In the Pt_2CdSe_3/Pt_2HgSe_3 heterostructure studied here, only time-reversal symmetry is present, leading to nonzero $\mathbf{\Omega}(\mathbf{k})$. We calculated $\Omega_z(\mathbf{k})$ for the Pt_2CdSe_3/Pt_2HgSe_3 bilayer for different values of applied electric field. In all cases, as shown in Fig. 5 [and also in Figs. S5(a)– S5(c) in SM [60]], they are finite, with the same magnitude and opposite signs in each valley, with opposite spin splittings. It is seen that for fields in the positive z direction, the external field acts to compensate to a degree the effect of a lack of inversion symmetry in the system, as the Berry curvature is reduced by an order of magnitude, whereas for an electric field in the opposite direction that compensation effect does not occur. Interestingly, for the case of an electric field of $E_{\hat{z}} = +0.5$ V/Å, the sign of the Berry curvature changes at the vicinity of the K and K' points in comparison with the zero-field case, whereas in the surrounding region in momentum space the sign remains unchanged.

When two single layers of a QSH semiconductor or insulator are combined to form a heterobilayer system in the limit of weak interlayer coupling, its $\mathbb{Z}_2$ invariant vanishes

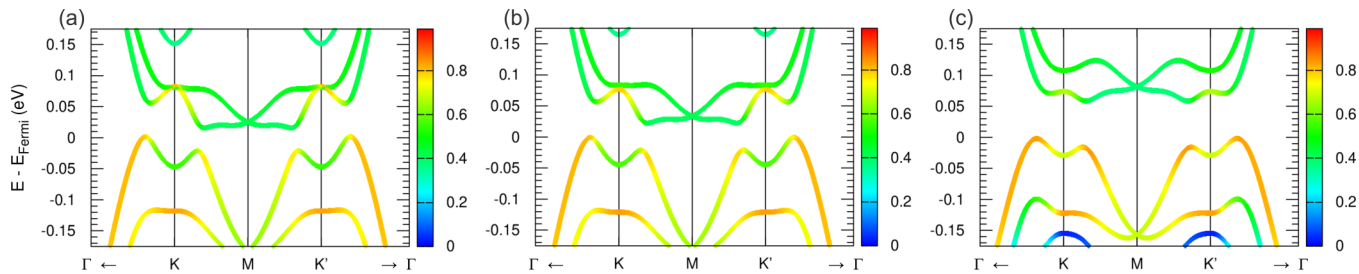

FIG. 4. Projection Pt_2CdSe_3 layer for the band structure for heterobilayer Pt_2CdSe_3/Pt_2HgSe_3 with an electric field (a) $E_{\hat{z}} = -0.5$ V/Å, (b) $E_{\hat{z}} = 0.0$ V/Å, and (c) $E_{\hat{z}} = +0.5$ V/Å.

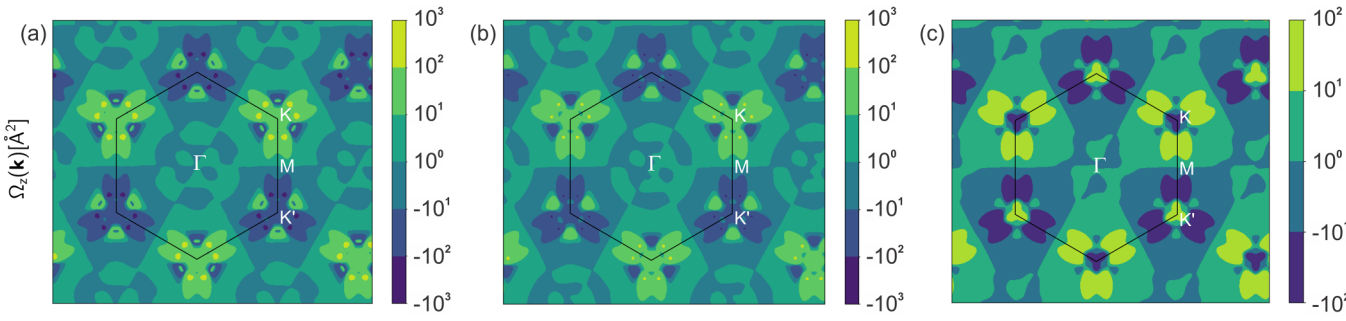

FIG. 5. Berry curvature for a Pt_2CdSe_3/Pt_2HgSe_3 heterostructure electric field (a) $E_{\hat{z}} = -0.5$ V/Å, (b) $E_{\hat{z}} = 0.0$ V/Å, and (c) $E_{\hat{z}} = +0.5$ V/Å.

and the system becomes topologically trivial [61]. The same behavior is expected for the case of homobilayers. In the case of heterobilayers, the symmetry group of the system formed can lead to the destruction or emergence of new topological states and the electronic particularity of each layer can lead to sufficiently strong interlayer interactions avoiding triviality. In this work, hybrid Wannier center calculations confirmed that the combination results in a nontopological system. For the range of applied electric fields no QSH-like topological transition was observed. Nevertheless, valley contrasting at the K and K' points in the nonzero Berry curvature in the Pt_2CdSe_3/Pt_2HgSe_3 heterobilayer reveals a QVH signature, independent of the presence of the electric field [17,20].

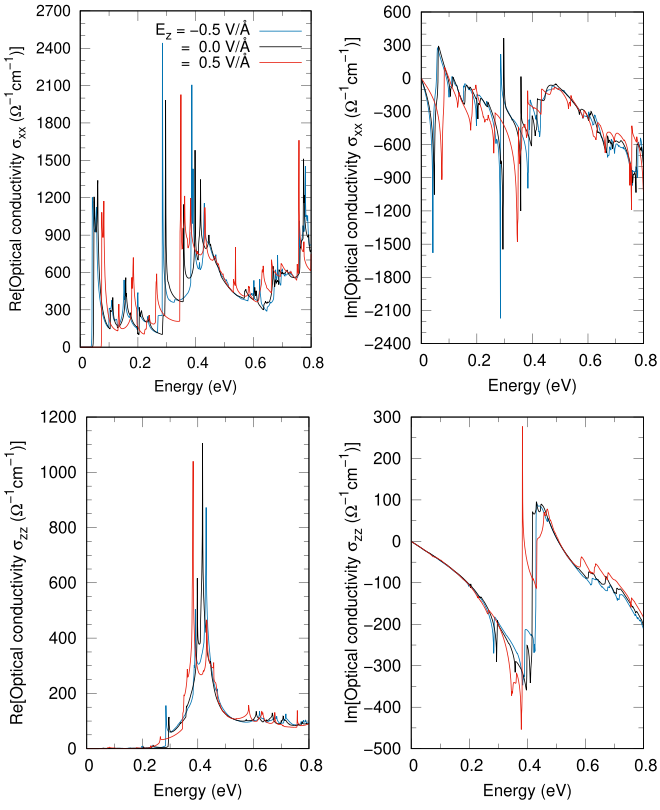

FIG. 6. Real and imaginary parts of the symmetric tensor of the optical conductivity for a Pt_2CdSe_3/Pt_2HgSe_3 heterobilayer.

In Fig. 6 we present the optical conductivity for the case with and without a perpendicular electric field applied. The real part of the optical conductivity is a measure of the optical absorption. A strong anisotropy is seen when one compares the tensor components σ_{xx} and σ_{zz}. A significant difference in the profile and intensity peaks is a larger in-plane absorption, which is approximately twice as large as the absorption in the out-of-plane direction. For the latter case, it is only possible for a frequency threshold of energy more than 0.2 eV, while for the in-plane absorption it is slightly larger than the electronic gap. Furthermore, the out-of-plane optical absorption edge is blueshifted with respect to its in-plane counterpart, considering the same applied electric field which also affects both intensities and peak positions. The same blueshifted displacement happens with the imaginary part. This effect also can be observed in other 2D materials [62].

The application of $+0.5$ V/Å electric field yields in opposite trends in the in-plane and out-of-plane components of real optical conductivities, while the in-plane absorption edge is blueshifted, and its out-of-plane counterpart is redshifted and softened. This condition is also accompanied by a pronounced enhancement of the imaginary part of the optical conductivity at 0.38 eV. These effects emerge from the influence of the external electric field on the electronic band structure of the heterostructure, changing the fine features of the electronic bands, their energy levels, and the oscillator strengths associated with the transitions.

IV. CONCLUSION

In this paper, we studied the influence of the electric field on the electronic properties, Berry curvature, and optical conductivity of a PtCdSe/PtHgSe van der Waals heterobilayer by means of first-principles calculations and MLWFs. The results showed that the influence of the electric field competes with the interlayer interactions, depending on the orientation of the electric field. For zero field the Pt_2CdSe_3/Pt_2HgSe_3 heterobilayer presents a band gap of 23 meV. The change in gap is significantly smaller when the electric field is applied in the $-\hat{z}$ direction as compared to the $+\hat{z}$ direction (15 meV vs 60 meV). The spin configuration in the valleys is maintained, however, the sign of the Berry curvature around the K and K' points is inverted with the application of the perpendicular electric field in opposite directions, but in the surrounding regions the sign is unchanged. The Berry curvature shows a QVH signature due to the presence of valley contrast and due

to the sizable band gap in the valley region. This ability to manipulate the Berry curvature around each valley can thus be relevant for applications in valleytronics, which seeks to encode information on the valley degrees of freedom of the system. Furthermore, we found a strong anisotropy in optical conductivity, where the out-of-plane optical absorption edge is blueshifted with respect to its in-plane counterpart and the application, and absorption is significantly concentrated in plane.

ACKNOWLEDGMENTS

This work was financially supported by the Brazilian Council for Research (CNPq, Grant No. 144332/2019-1).

[1] N. R. Glavin, R. Rao, V. Varshney, E. Bianco, A. Apte, A. Roy, E. Ringe, and P. M. Ajayan, Adv. Mater. **32**, 1904302 (2020).
[2] P. Ares and K. S. Novoselov, Nano Mater. Sci. **4**, 3 (2022).
[3] B. Guo, Q.-l. Xiao, S.-h. Wang, and H. Zhang, Laser Photonics Rev. **13**, 1800327 (2019).
[4] J. Nan, X. Guo, J. Xiao, X. Li, W. Chen, W. Wu, H. Liu, Y. Wang, M. Wu, and G. Wang, Small **17**, 1902085 (2021).
[5] A. Gupta, T. Sakthivel, and S. Seal, Prog. Mater. Sci. **73**, 44 (2015).
[6] S. Balendhran, S. Walia, H. Nili, S. Sriram, and M. Bhaskaran, Small **11**, 640 (2015).
[7] A. H. Castro Neto, F. Guinea, N. M. R. Peres, K. S. Novoselov, and A. K. Geim, Rev. Mod. Phys. **81**, 109 (2009).
[8] G. R. Bhimanapati, Z. Lin, V. Meunier, Y. Jung, J. Cha, S. Das, D. Xiao, Y. Son, M. S. Strano, V. R. Cooper *et al.*, ACS Nano **9**, 11509 (2015).
[9] M. Z. Hasan and C. L. Kane, Rev. Mod. Phys. **82**, 3045 (2010).
[10] J. Cayssol and J. N. Fuchs, J. Phys.: Mater. **4**, 034007 (2021).
[11] A. Bansil, H. Lin, and T. Das, Rev. Mod. Phys. **88**, 021004 (2016).
[12] D. Xiao, M.-C. Chang, and Q. Niu, Rev. Mod. Phys. **82**, 1959 (2010).
[13] V. Bhardwaj and R. Chatterjee, Resonance **25**, 431 (2020).
[14] T. Olsen, E. Andersen, T. Okugawa, D. Torelli, T. Deilmann, and K. S. Thygesen, Phys. Rev. Mater. **3**, 024005 (2019).
[15] D. Vanderbilt, *Berry Phases in Electronic Structure Theory* (Cambridge University Press, Cambridge, U.K., 2018).
[16] A. Isaeva, B. Rasche, and M. Ruck, Phys. Status Solidi RRL **7**, 39 (2013).
[17] W. Yao, D. Xiao, and Q. Niu, Phys. Rev. B **77**, 235406 (2008).
[18] X.-L. Zhang, L. Xu, and J. Zhang, J. Phys.: Condens. Matter **29**, 185502 (2017).
[19] K. Komatsu, Y. Morita, E. Watanabe, D. Tsuya, K. Watanabe, T. Taniguchi, and S. Moriyama, Sci. Adv. **4**, eaaq0194 (2018).
[20] S. Sinha, P. C. Adak, R. Surya Kanthi, B. L. Chittari, L. Sangani, K. Watanabe, T. Taniguchi, J. Jung, and M. M. Deshmukh, Nat. Commun. **11**, 5548 (2020).
[21] B. A. Bernevig, T. L. Hughes, and S.-C. Zhang, Science **314**, 1757 (2006).
[22] M. Xu, T. Liang, M. Shi, and H. Chen, Chem. Rev. **113**, 3766 (2013).
[23] F. C. de Lima, R. H. Miwa, and A. Fazzio, Phys. Rev. B **102**, 235153 (2020).
[24] A. Cabral, H. Galbiatti, R. Kwitko-Ribeiro, and B. Lehmann, Terra Nova **20**, 32 (2008).
[25] A. Vymazalová, F. Laufek, M. Drábek, A. R. Cabral, J. Haloda, T. Sidorinová, B. Lehmann, H. F. Galbiatti, and J. Drahokoupil, Can. Mineral. **50**, 431 (2012).
[26] R. Longuinhos, A. Vymazalová, A. R. Cabral, S. S. Alexandre, R. W. Nunes, and J. Ribeiro-Soares, J. Raman Spectrosc. **51**, 357 (2020).
[27] A. Marrazzo, M. Gibertini, D. Campi, N. Mounet, and N. Marzari, Phys. Rev. Lett. **120**, 117701 (2018).
[28] K. Kandrai, P. Vancsó, G. Kukucska, J. Koltai, G. Baranka, Á. Hoffmann, Á. Pekker, K. Kamarás, Z. E. Horváth, A. Vymazalová *et al.*, Nano Lett. **20**, 5207 (2020).
[29] J. I. Facio, S. K. Das, Y. Zhang, K. Koepernik, J. van den Brink, and I. C. Fulga, Phys. Rev. Mater. **3**, 074202 (2019).
[30] I. Cucchi, A. Marrazzo, E. Cappelli, S. Riccò, F. Y. Bruno, S. Lisi, M. Hoesch, T. K. Kim, C. Cacho, C. Besnard, E. Giannini, N. Marzari, M. Gibertini, F. Baumberger, and A. Tamai, Phys. Rev. Lett. **124**, 106402 (2020).
[31] T.-N. Do, G. Gumbs, P.-H. Shih, D. Huang, C.-W. Chiu, C.-Y. Chen, and M.-F. Lin, Sci. Rep. **9**, 624 (2019).
[32] M. U. Rehman, Z. Qiao, and J. Wang, Phys. Rev. B **105**, 165417 (2022).
[33] M. U. Rehman, M. Kiani, and J. Wang, Phys. Rev. B **105**, 195439 (2022).
[34] T. Hesjedal and Y. Chen, Nat. Mater. **16**, 3 (2017).
[35] A. K. Geim and I. V. Grigorieva, Nature (London) **499**, 419 (2013).
[36] W. Wang, S. Dai, X. Li, J. Yang, D. J. Srolovitz, and Q. Zheng, Nat. Commun. **6**, 7853 (2015).
[37] K. Novoselov, A. Mishchenko, A. Carvalho, and A. Castro Neto, Science **353**, aac9439 (2016).
[38] A. Bafekry, M. Obeid, C. V. Nguyen, M. Ghergherehchi, and M. B. Tagani, J. Mater. Chem. A **8**, 13248 (2020).
[39] Z. Liu, Y. Han, Y. Ren, Q. Niu, and Z. Qiao, Phys. Rev. B **104**, L121403 (2021).
[40] P. Hohenberg and W. Kohn, Phys. Rev. **136**, B864 (1964).
[41] W. Kohn and L. J. Sham, Phys. Rev. **140**, A1133 (1965).
[42] P. Giannozzi, S. Baroni, N. Bonini, M. Calandra, R. Car, C. Cavazzoni, D. Ceresoli, G. L. Chiarotti, M. Cococcioni, I. Dabo *et al.*, J. Phys.: Condens. Matter **21**, 395502 (2009).
[43] P. Giannozzi, O. Andreussi, T. Brumme, O. Bunau, M. B. Nardelli, M. Calandra, R. Car, C. Cavazzoni, D. Ceresoli, M. Cococcioni *et al.*, J. Phys.: Condens. Matter **29**, 465901 (2017).
[44] R. Fletcher, *Practical Methods of Optimization* (Wiley, New York, 1987).
[45] S. R. Billeter, A. J. Turner, and W. Thiel, Phys. Chem. Chem. Phys. **2**, 2177 (2000).
[46] S. R. Billeter, A. Curioni, and W. Andreoni, Comput. Mater. Sci. **27**, 437 (2003).
[47] T. Sohier, M. Calandra, and F. Mauri, Phys. Rev. B **96**, 075448 (2017).
[48] J. P. Perdew, K. Burke, and M. Ernzerhof, Phys. Rev. Lett. **77**, 3865 (1996).

[49] A. Tkatchenko and M. Scheffler, Phys. Rev. Lett. **102**, 073005 (2009).
[50] D. R. Hamann, Phys. Rev. B **88**, 085117 (2013).
[51] M. J. van Setten, M. Giantomassi, E. Bousquet, M. J. Verstraete, D. R. Hamann, X. Gonze, and G.-M. Rignanese, Comput. Phys. Commun. **226**, 39 (2018).
[52] A. A. Mostofi, J. R. Yates, Y.-S. Lee, I. Souza, D. Vanderbilt, and N. Marzari, Comput. Phys. Commun. **178**, 685 (2008).
[53] A. A. Mostofi, J. R. Yates, G. Pizzi, Y.-S. Lee, I. Souza, D. Vanderbilt, and N. Marzari, Comput. Phys. Commun. **185**, 2309 (2014).
[54] G. Pizzi, V. Vitale, R. Arita, S. Blügel, F. Freimuth, G. Géranton, M. Gibertini, D. Gresch, C. Johnson, T. Koretsune *et al.*, J. Phys.: Condens. Matter **32**, 165902 (2020).
[55] Q. Wu, S. Zhang, H.-F. Song, M. Troyer, and A. A. Soluyanov, Comput. Phys. Commun. **224**, 405 (2018).
[56] I. Souza, N. Marzari, and D. Vanderbilt, Phys. Rev. B **65**, 035109 (2001).
[57] X. Wang, J. R. Yates, I. Souza, and D. Vanderbilt, Phys. Rev. B **74**, 195118 (2006).
[58] J. R. Yates, X. Wang, D. Vanderbilt, and I. Souza, Phys. Rev. B **75**, 195121 (2007).
[59] T. Zhou, J. Zhang, B. Zhao, H. Zhang, and Z. Yang, Nano Lett. **15**, 5149 (2015).
[60] See Supplemental Material at http://link.aps.org/supplemental/10.1103/PhysRevB.107.085418 for the mentioned supplemental results.
[61] H. Pan, X. Li, Z. Qiao, C.-C. Liu, Y. Yao, and S. A. Yang, New J. Phys. **16**, 123015 (2014).
[62] I. Guilhon, M. Marques, L. K. Teles, M. Palummo, O. Pulci, S. Botti, and F. Bechstedt, Phys. Rev. B **99**, 161201(R) (2019).